DOI: 10.1002/ejic.200800658

Magnetic Properties of $Ni^{II}Cr^{III}$ Layered Double Hydroxide Materials

Juan J. Almansa,[a] Eugenio Coronado,*[a] Carlos Martí-Gastaldo,[a] and Antonio Ribera*[a]

Dedicated to Prof. Jan Reedijk on the occasion of his 65th birthday

Keywords: Layered compounds / Chromium / Nickel / Magnetic properties / Spin frustration

This paper describes the isolation of four layered double hydroxide (LDH) compounds having the general formula $[Ni^{II}_{3-x}Cr^{III}_{x}(OH)_6](CO_3)_{x/2}{\cdot}yH_2O$ [x = 0.57 (**1**), 0.69 (**2**), 0.81 (**3**) and 0.93 (**4**)] by using homogeneous precipitation methods and varying the metal ratio in the synthetic solutions. All the reported compounds have carbonate anions in the interlamellar space. This fact forces the interlayer distances to remain unchanged in all the cases, thus providing an ideal system in which the changes observed in magnetic properties can be correlated with metal composition along the hydroxide layers.

Introduction

Since the mid-19th century, when the natural mineral hydrotalcite was discovered in Sweden, a large list of natural and synthetic layered double hydroxides (LDHs) has been described. LDHs are a class of anionic clays whose structure is related to that of brucite, $Mg(OH)_2$, in which some of the divalent cations have been randomly substituted with trivalent ions, giving rise to positively charged sheets. They present the general formula $[M^{II}_{3-x}M^{III}_{x}(OH)_6](A^{n-})_{x/n}{\cdot}yH_2O$,[1] in which the identities of the divalent and trivalent cations (M^{II} and M^{III} respectively), the nature of the interlayer anion (A^{n-}) and the value of the stoichiometric coefficient x ($0.60 \leq x \leq 1$) may be varied over a wide range to obtain a large number of LDH materials. Electrostatic interactions between positively charged brucite layers and the interlaminar anions are the main feature responsible for the pillaring in the solid state. A variable amount of water molecules are also intercalated in the interlamellar space resulting from hydrogen bonding interactions with hydroxyl groups pointing outside the cationic layers.

These layered compounds have been recently used to prepare novel hybrid materials. Thus, by taking advantage of the ability of the intercalated anion to leave the interlayer space by means of soft chemistry methods, novel hybrid materials, whose properties result from the combination of those presented by the LDH inorganic template and the anionic species, have been prepared. By following this strategy, relatively simple anionic molecules (CO_3^{2-}, Cl^-, I^- or NO_3^-) intercalated in the synthetic process have been replaced by more complex molecular species as, for example, phthalocyanine and metalloporphyrin derivatives,[2] polyoxometalates,[3] biomolecules[4] or pharmaceutical agents.[5]

Despite the increasing interest raised by this sort of lamellar compounds, to the best of our knowledge, the magnetic properties of dimetallic LDHs have been poorly described. Antiferromagnetic interactions within the plane were observed at low temperature for the family $[Cu_{3-x}Al_x(OH)_6](A^{n-})_{x/n}{\cdot}yH_2O$ (A = CO_3^{2-} or alkylsulfonate anion).[6] Nevertheless, no signature of spontaneous magnetization was observed down to 2 K. Magnetic measurements were also performed on the $[Co_2Fe_yAl_{1-y}(OH)_6]Cl{\cdot}nH_2O$ family of materials.[7] The interlayer spacing in these compounds was modulated from 7.6 up to 25 Å by using surfactant molecules with the aim of studying the effect of interlayer spacing on the resulting magnetic properties. Preliminary results indicated that both intralayer magnetic coupling and interlayer separation affected interlayer dipolar interactions. Still, these results did not lead to the conclusion that long-range magnetic ordering existed.

In contrast to LDHs, homometallic hydroxides have been extensively studied. Indeed, magneto-structural correlations have been established in the family of hybrid compounds $[M^{II}_2(OH)_3](X)$ (M^{II} = Cu, Co; X^- = anionic organic linker).[8] Several members of this family undergo magnetic ordering with appearance of spontaneous magnetization at temperatures as high as 40 K, as result of hydroxyl-mediated superexchange between paramagnetic ions along the 2D layers and interplane dipolar interactions. Large coercive fields, driven by the synergy of crystalline shape and

[a] Instituto de Ciencia Molecular, Universidad de Valencia, Polígono de la Coma s/n 46980, Paterna (Valencia), Spain
Fax: +34-963523273
E-mail: eugenio.coronado@uv.es

Supporting information for this article is available on the WWW under http://www.eurjic.org/ or from the author.

single-ion anisotropies as well as the perpendicular alignment of the spins with respect to the layers, have also been observed.[9]

The scarcity of studies describing the magnetic properties of dimetallic LDH systems, relative to those concerning layered homometallic hydroxides,[8,9] is certainly related to the larger structural and magnetic complexity of the former. In this case, a random distribution of the paramagnetic metals along the hydroxide layer might lead to the occurrence of three different magnetic interactions between M^{II} and M^{III} nearest-neighbours: M^{II}–O–M^{II}, M^{II}–O–M^{III} and M^{III}–O–M^{III}, which could be in competition. In this context, Bujoli-Deouff et al. described the static magnetic properties of a family of $Ni^{II}Cr^{III}$ hydroxide-based 2D materials by changing the Cr/(Ni+Cr) molar ratio in the cationic layers in the 0.25–0.50 range.[10] In view of the fact that pure crystalline phases of LDH systems could only be obtained in the 0.2–0.33 composition range,[1a] we have prepared and magnetically characterized only those systems satisfying this requirement. In addition, whereas the traditional co-precipitation method was employed in the former work, a homogeneous precipitation method has now been applied. The utilization of an ammonia-releasing reagent like urea allows highly crystalline LDH systems exhibiting well-defined morphologies to be obtained.

With the aim of examining the relevance of dimetallic LDHs in magnetism, we are undertaking an extensive program which includes the preparation of new layered magnets of this family, along with the preparation of new hybrid magnets obtained by intercalation of magnetic molecular species in between the magnetic LDHs.[11] Here we describe the synthesis and physical characterization of a family of layered magnets based on NiCr LDHs. By using homogeneous precipitation methods and varying the metal ratio in the synthetic solutions, we succeeded in the isolation of four compounds described by the general formula $[Ni^{II}_{3-x}Cr^{III}_{x}(OH)_6](CO_3)_{x/2}\cdot yH_2O$ [x = 0.57 (**1**), 0.69 (**2**), 0.81 (**3**) and 0.93 (**4**)]. All the reported compounds have carbonate anions in the interlamellar space. Subsequently, the interlayer distances are kept unchanged in all the cases, thus providing an ideal system for correlating the changes observed in magnetic properties with metal composition along the hydroxide layers.

Results and Discussion

Synthesis

LDHs have been most commonly prepared by coprecipitation from aqueous solutions of the metal salts by adding a NaOH solution, while maintaining the pH slightly alkaline and the temperature high in order to increase their crystallinity.[12] Nevertheless, this method led to poorly crystallized solids. Recently, LDHs presenting uniform size and well-defined hexagonal shape have been prepared by so-called "*homogeneous precipitation methods*". In such methods, the ammonia generated by the hydrolysis of "*ammonia-releasing reagents*" (ARRs), such as urea and hexamethylenetetramine (HMT), makes it possible to increase the pH slowly in order to induce the slow precipitation of the resulting LDH materials.[13] We have used this second approach to prepare the compounds $[Ni^{II}_{3-x}Cr^{III}_{x}(OH)_6](CO_3)_{x/2}\cdot yH_2O$ [x = 0.57 (**1**), 0.69 (**2**), 0.81 (**3**) and 0.93 (**4**)]. In a typical SEM image (Figure 1, right), hexagonal platelets with a lateral size of approximately 20 μm together with small and more irregular crystals can be observed for all samples except for **1**. For this compound, the crystal shape is more irregular (Figure 1, left), and no hexagonal platelet can be clearly distinguished. Nevertheless, all the compounds (**1**–**4**) show the typical platelet shape of the LDH crystals when prepared by homogeneous precipitation methods, in contrast to the so-called "sand rose morphology" observed when high base supersaturation conditions are employed.

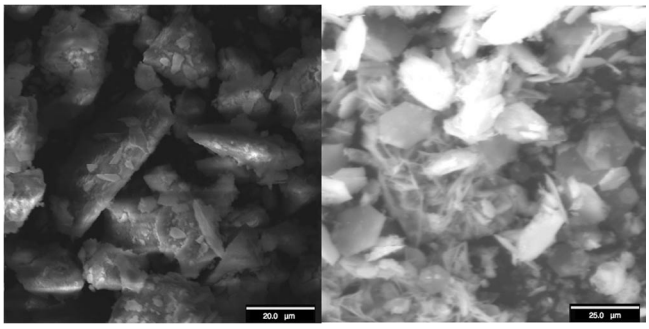

Figure 1. SEM images of **1** (left) and **4** (right). The morphology exhibited by compounds **2** and **3** (see Figure S1) was very similar to that observed for **4**.

The metal composition of the as-prepared bulk samples was determined by means of electron probe microanalysis. Table 1 shows the content of transition metal ions in the synthetic solution together with those found in the isolated materials. Experimental x values are slightly lower than those corresponding to the synthetic mixture.

Table 1. Metal ratio employed in the experimental solutions and found in the isolated compounds, water content derived from thermogravimetric analysis and estimated molecular formula for compounds **1**–**4**.

	x		Water content		Molecular formula
	Exp.	Theor.	Wt.-%	Mol	
1	0.57	0.6	20.76	4.14	$[Ni_{2.43}Cr_{0.57}(OH)_6](CO_3)_{0.29}]\cdot(H_2O)_{4.14}$
2	0.69	0.75	18.60	3.70	$[Ni_{2.30}Cr_{0.69}(OH)_6](CO_3)_{0.35}]\cdot(H_2O)_{3.70}$
3	0.81	0.9	17.56	3.48	$[Ni_{2.19}Cr_{0.81}(OH)_6](CO_3)_{0.41}]\cdot(H_2O)_{3.48}$
4	0.93	1	14.79	2.89	$[Ni_{2.07}Cr_{0.93}(OH)_6](CO_3)_{0.47}]\cdot(H_2O)_{2.89}$

Structural Characterization

This information has been extracted form FTIR spectroscopy and X-ray powder diffraction analysis. FTIR spectroscopy is a very useful technique in the study of LDH compounds. It allows not only the identification of molecules intercalated in the LDH interlamellar space but also the determination of their orientation with respect to the brucite-like sheets. Important information about the nature

and intensity of the interactions of the anions with the neighbouring hydroxido groups can also be extracted. Figure S2 shows the FTIR spectra recorded for compounds **1**–**4**. The assignment of vibration modes is summarized in Table S3. The broad intense lines observed between 3416–3388 cm^{-1} can be ascribed to the O–H stretching vibration mode of water molecules intercalated within the interlamellar space. Besides interlamellar water molecules, hydrogen-bonded hydroxyl groups along the cationic sheets might also be responsible for the observed band broadening.[1a] The medium intensity band around 1630 cm^{-1} is related to the bending mode of hydrogen-bonded water molecules. In fact, the intensity of this band is proportional to the amount of intercalated water in the studied sample. The stretching mode (ν_3) of CO_3^{2-} anions is responsible for the sharp strong band around 1360 cm^{-1}.[14] Stretching and bending vibrational modes attributed to hydroxometallic octahedral complexes constituting the $[Ni^{II}_{3-x}Cr^{III}_x(OH)_6]^{x+}$ cationic brucite-like sheets are responsible for absorption at lower wavenumbers.[14,15]

X-ray diffraction patterns obtained for compounds **1**–**4** are shown in Figure 2. They present the expected profile for LDH compounds, confirming the phase purity for all the isolated materials. Sharp intense diffraction peaks can be observed at low 2θ values, while they become broader and weaker at higher angles. The characteristic sharp diffraction harmonic peaks can be indexed as (00*l*) reflections by assuming rhombohedral 3*R* symmetry.[1a] Since these peaks are related to the stacking periodicity of the $[M^{II}_{3-x}M^{III}_x(OH)_6]^{x+}$ layers along the *c*-axis, they allowed us to estimate the basal spacing (BS) and the corresponding *c*-axis value (see Table 2). The broad peak around 60° can be indexed as (110) with respect to the hexagonal axes, and it is related to the size of the metal hydroxide layer along the *ab* plane, which allows us to estimate the *a*-axis value. The cell parameters other than the basal spacing for all the synthesized compounds are in excellent agreement with those previously reported for analogous LDH materials having intercalated CO_3^{2-} anions.[1a] Although all the diffraction patterns appear to be identical, confirming the LDH structure for all the reported compounds, that corresponding to compound **1** presents poorly defined peaks, which are broader than those of the other reported compounds. This fact might be attributed to the lower chromium(III) content ($x = 0.57$) in compound **1**. Indeed, many experimental indicators show that pure phase LDH materials can only be obtained when the experimental $0.6 \leq x \leq 1$ constraint is satisfied.[16] For *x* values below this range, the density of $Ni(OH)_6$ octahedra in the brucite-like layers is high. This situation favours the formation of amorphous $Ni(OH)_2$ through condensation, not detectable by X-ray measurements, thus leading to a poorly defined X-ray diffraction pattern.[17] The lower chromium(III) content of **1** can also account for the larger *a* value. Indeed, taking into account that the Cr^{III}–O distance is shorter than that of Ni^{II}–O, lower chromium(III) contents should yield larger *a* values.[18] The bigger basal spacing (BS) observed for this same compound must be also attributed to the different Ni/Cr metal ratio. As a result of the lower chromium(III) content, the positive charge supported by the brucite-like sheets is smaller. Therefore, the electrostatic forces between the cationic layers and the anionic molecules within the interlaminar space, responsible for the pillaring of the LDH material in the solid state, must be less intense, thus shrinking the *c* axis.[19]

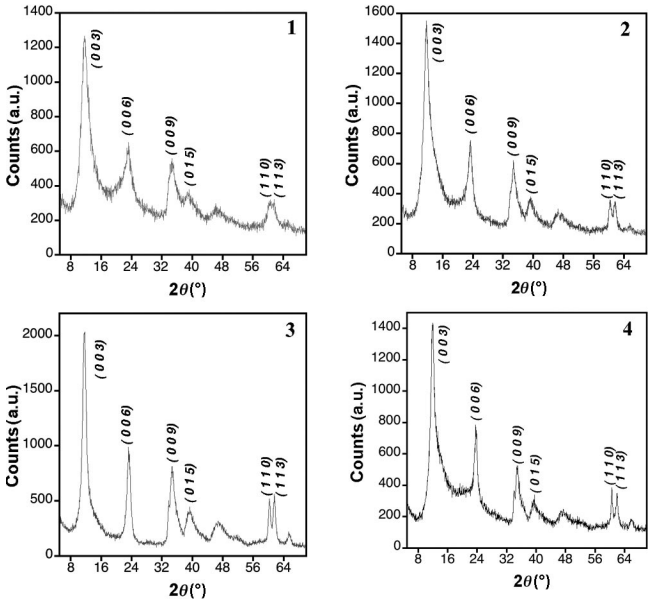

Figure 2. X-ray diffraction pattern for compounds **1**–**4**.

Table 2. X-ray diffraction pattern indexation and estimated parameters for compounds **1**–**4**.

	2θ (°) (*hkl*)				Estimated parameters (Å)			
	(003)	(006)	(009)	(110)	$d_{(110)}$	a[a]	c[b]	BS[c]
1	11.53	23.22	34.58	60.28	1.54	3.07	23.1	7.7
2	11.53	23.33	34.67	60.28	1.54	3.07	23.03	7.68
3	11.69	23.11	34.67	60.21	1.54	3.07	23.04	7.68
4	11.89	23.50	34.83	60.50	1.53	3.06	22.76	7.59

[a] $a = 2d_{(110)}$. [b] $c = [d_{(003)} + 2d_{(006)} + 3d_{(009)}]/3$. [c] BS = $c/3$.

Thermal Decomposition

Thermal behaviour of the isolated compounds was studied in the interval 25–800 °C in air (see Figure S3). Analogous TG and DTA curves were obtained in each case. As expected for LDH materials, the weight loss is due to a two-step process.[1a,20] The first low-temperature weight loss, in the 25–220 °C range, is attributed to the removal of water molecules located in the interlaminar space and does not promote a structural collapse. The higher-temperature weight-loss process, which occurs from 220 to 800 °C, is mainly promoted by loss of carbonate anions and further dehydroxylation of $[Ni^{II}_{3-x}Cr^{III}_x(OH)_6]^{x+}$ brucite-like sheets. DTA profiles recorded for compounds **1**–**3** (see Figure S4) show a high-intensity, well-defined endothermic peak in the 60–65 °C interval in addition to two poorly defined shoulders above 220 °C. The low-temperature peak

can be ascribed to the first-step weight loss, while the rest of the endothermic signals must be attributed to the higher-temperature process. Compound **4** presents better resolved endothermic peaks at temperatures very close to those observed for its counterparts.

Although we did not monitor the gas evolution during the thermal decomposition of the samples, according to previously reported studies, the water content was calculated on the basis of the low-temperature weight-loss step.[21] From the resulting values, we observe that the amount of water in the interlayer space decreases with increasing x values. In fact, the higher charge density supported by the hydroxide layers must be balanced by a higher amount of CO_3^{2-} anions, thus resulting in smaller c-axis values and a lower amount of intercalated water molecules.

Magnetic Properties

According to the structure of LDH materials (2D layers composed of metallic octahedral sharing edges), superexchange must occur through the oxido bridges linking neighbouring $M^{II,III}(OH)_6$ units. Although metal ions are expected to be randomly distributed in the LDH sheets, they will be statistically distributed in a ratio fixed by their molecular formula. For example, in a NiCr compound with a 2:1 metal ratio (x = 1), each Cr^{3+} ion will be statistically surrounded by six Ni^{2+} ions (Ni–O–Cr pairs), while each Ni^{2+} atom will be neighboured by three Cr^{3+} and three Ni^{2+} ions (Ni–O–Ni pairs). We would like to indicate that the probability of the presence of Cr–O–Cr pairs throughout the layers is very low but cannot be ignored. For the Ni–O–Ni pairs, orthogonality between the e_g magnetic orbitals of octahedral Ni^{2+} ions should promote ferromagnetic exchange. Indeed, ferromagnetic ordering in both the brucite-like $Ni(OH)_2$[22] and the $[Ni_2Al(OH)_6](NO_3)$ layered double hydroxide[23] have been observed. On the contrary, Cr–O–Cr pairs should promote antiferromagnetic (AF) exchange since overlap between the t_{2g} magnetic orbitals of octahedral Cr^{3+} ions cannot be avoided. AF coupling is also expected for the Ni–O–Cr pairs, as a result of the overlap between the Ni^{2+} e_g and Cr^{3+} t_{2g} magnetic orbitals. In the four reported compounds, x remains in the range 0.57–0.93. Thus, **2** (x = 0.69), **3** (x = 0.81) and **4** (x = 0.93) can be considered as derivatives of **1** (x = 0.57) in which certain Ni^{2+} positions have been substituted by Cr^{3+} ions. This substitution will cause a change in the number of ferromagnetic Ni–O–Ni and antiferromagnetically coupled Ni–O–Cr or Cr–O–Cr pairs all over the layers, therefore modifying the overall intralayer magnetic exchange. Taking into account that the interlamellar distance is almost constant for all studied compounds (ca. 7.7 Å), the extent of interlayer magnetic coupling operating through dipolar interactions is expected to be nearly the same for all of them. In this way, the major differences observed in their magnetic behaviour must be attributed to the net intralayer magnetic exchange.

Measurements of dc susceptibility at 1000 G were performed on compounds **1**–**4**. The $\chi_M T$ vs. T plot shows a similar profile for all of them (Figure 3). Upon cooling from room temperature down to 60 K, the $\chi_M T$ value remains almost constant. Below 60 K, the signal starts increasing smoothly down to 30 K when this increase becomes abrupt, defining a maximum (62.8, 73.2, 73.1 and 50.9 emu K mol^{-1} for **1**, **2**, **3** and **4**, respectively) at around 15 K, which corresponds to a steep jump in the χ_M signal, suggesting the appearance of a long-range correlated magnetic state. Magnetic data were fitted into the Curie–Weiss law in the high-temperature regime (150–300 K; see Figure S5). They yielded negative Weiss temperatures (Θ) and Curie constant values (C) of 3.32, 3.33, 3.47 and 3.65 emu K mol^{-1} for **1**, **2**, **3** and **4** respectively (see Table 3). These C values are in excellent agreement with those expected for a magnetically diluted combination of Ni^{2+} (S = 1) and Cr^{3+} (S = 3/2) ions in the ratio previously determined by electron probe microanalysis. The obtained negative Θ values are indicative of the presence of overall antiferromagnetic interactions between spin carriers in the hydroxide-based sheets. Note that Θ becomes more negative as the amount of Cr^{3+} ions in the 2D layer increases (–1.31, –3.52, –4.64, –9.84 K for **1**, **2**, **3** and **4**, respectively). This trend is supported by the higher ratio of antiferromagnetically coupled Ni–O–Cr and Cr–O–Cr pairs with respect to the ferromagnetic Ni–O–Ni ones. These magnetic properties are summarized in Table 3.

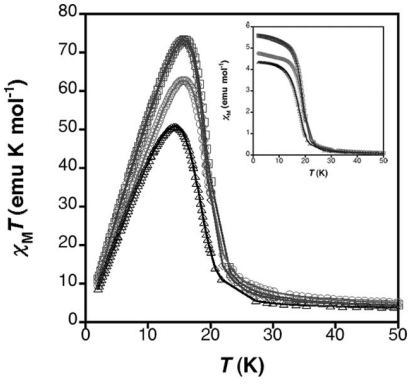

Figure 3. Temperature dependence of the $\chi_M T$ product for **1** (circles), **2** (squares), **3** (diamonds) and **4** (triangles) in the low-temperature regime. The inset shows the low-temperature χ_M vs. T plot.

Table 3. Magnetic parameters for **1**–**4**: expected spin-only value of the Curie constant [C_{so}, (emu K mol^{-1})], experimental Curie constant [C, (emu K mol^{-1})], Weiss constant (Θ), saturation magnetization (M_S), remnant magnetization at 2 K (M_R), coercive field at 2 K (H_{Coer}), critical temperature (T_c) and frequency-shift parameter (ϕ). $S(Cr^{3+})$ = 3/2, $S(Ni^{2+})$ = 1.

	C_{so}	C	Θ (K)	M_S (μ_B)	M_R (μ_B)	H_{Coer} (kG)	T_c (K)	ϕ
1	3.50	3.32	–1.31	2.52	1.04	5.4	19.5	0.042
2	3.60	3.33	–3.52	2.09	1.13	6.6	19.4	0.049
3	3.74	3.47	–4.64	1.87	1.06	11.3	20.6	0.010
4	3.81	3.65	–9.84	1.57	0.80	2.8	21	0.006

The predominance of antiferromagnetic interactions all over the $[Ni_{3-x}Cr_x(OH)_6]^{x+}$ layers is confirmed by the field dependence of the magnetization at low temperatures. The whole set of compounds exhibit a continuous increase in the magnetization from very low fields up to 5 T, reaching values (2.52, 2.09, 1.87, 1.57 μ_B) that are far from saturation, as expected for ferrimagnetic systems. Note that the magnetization values at high fields are lowered as the Cr^{3+} content in the brucite-like sheets is increased. This trend, equivalent to that previously observed in the Θ values, can be attributed to the ratio of AF/F coupled pairs. We would like to remark that for compounds **1**, **2** and **3** the magnetization curve shows a sigmoidal shape at low fields (see Figure 4). Hysteresis loops were observed for all the compounds, which confirms the occurrence of spontaneous magnetization at low temperatures. Coercive fields are in the range 11.3–2.8 kG; therefore, these materials can be classified as hard magnets (see Table 3 and Figure S6).

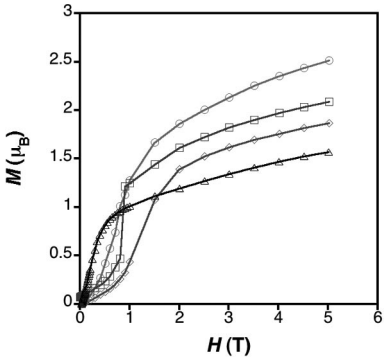

Figure 4. Field dependence of the magnetization at 2 K for **1** (circles), **2** (squares) **3** (diamonds) and **4** (triangles).

Measurements of ac dynamic susceptibility were performed under an oscillating applied field of 3.95 G. Both the in-phase (χ'_M) and the out-of-phase (χ''_M) signals define a peak at low temperatures, which confirms the occurrence of spontaneous magnetization in all of the cases. Critical temperatures (T_c), defined as the temperature where the χ''_M signal becomes nonzero, are in the 19.4–21 K interval (Figure 5). Below T_c, the χ''_M signal increases very rapidly upon cooling down with a positive slope, which is frequency-independent. At lower temperatures, χ''_M reaches a maximum, whose position exhibits strong frequency dependence. This dependence can be quantified with the frequency-shift parameter, ϕ, by using the expression firstly introduced by Mydosh:[24]

$$\phi = \Delta T_f/[T_f\,(\Delta \log \omega_i)]$$

where T_f is defined as the temperature corresponding to the maximum in the χ_M'' vs. T curve for each frequency value (ω_i), and ΔT_f corresponds to the difference between the T_f values for the minimum and maximum frequency. The obtained ϕ values, 0.042, 0.049, 0.010 and 0.006 for **1**, **2**, **3** and **4**, respectively, are in good agreement with those expected for spin glasses (typically $0.001 \leq \phi \leq 0.1$). Note that such frequency dependence might also be due to a movement of the domain walls in the ordered state. Furthermore, as expected for spin glasses, the fitting of the data frequency dependence into an Arrhenius law led to meaningless physical values for the energy barrier (Δ/k_B = 796, 700, 3550 and 5090 K for **1**, **2**, **3** and **4**, respectively, see Figure S7).

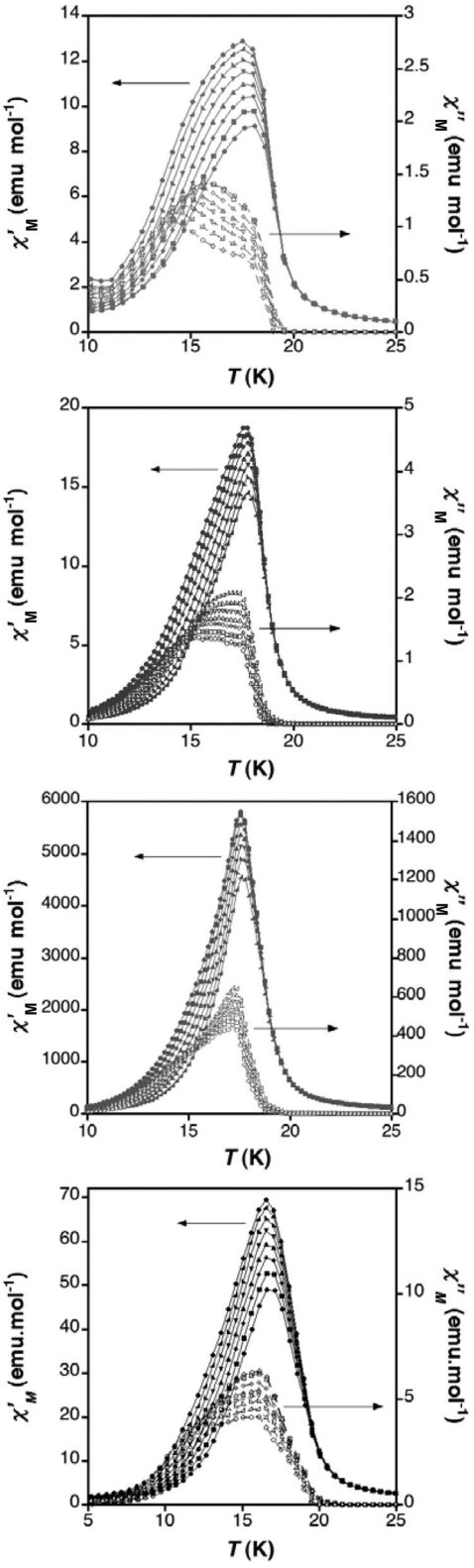

Figure 5. Measurements of ac susceptibility for the isolated compounds. Solid symbols represent in-phase signals and open symbols the out-of-phase signals (from top to bottom: **1**, **2**, **3** and **4**).

In summary, two contributions to the ac imaginary part can be extracted: a first high-temperature rapid increase in the χ''_M signal induced by the onset of a long-range ferrimagnetic ordered state (T_c) and a lower-temperature frequency-dependent maximum associated to the spin-glass transition (T_f). The main reasons for the appearance of spin-glass behaviour in magnetic materials are structural disorder and competing magnetic interactions. Although many examples describing glassy-like magnetic behaviour have already been reported, those describing a "reentrant" transition, where the magnetically ordered ferrimagnetic state reenters a disordered glassy state at lower temperature, are relatively few.[24,25] Taking into account that all the studied compounds show well-defined X-ray diffraction patterns, they must be considered to be polycrystalline solids and not amorphous materials. Hence, glassiness in this sort of compounds must arise from the coexistence of competing magnetic interactions and the random distribution of spin carriers throughout the hydroxide-supported cationic layers. Indeed, statistical disorder might induce the substitution of Ni^{2+} atoms with Cr^{3+} in certain positions of the 2D network. If we assume that only the nearest-neighbour magnetic interactions are significant, this substitution might generate spin frustration. Figure 6 shows how the substitution of a Ni^{2+} cation by a Cr^{3+} cation generates frustration in the former. Note that the spin of the central Cr^{3+} ion is antiferromagnetically coupled to the Ni^{2+} next-neighbours, whereas the spin of the inserted Cr^{3+} ion is frustrated because it wants to be antiferromagnetically coupled to the adjacent Ni^{2+} and Cr^{3+} spins simultaneously.

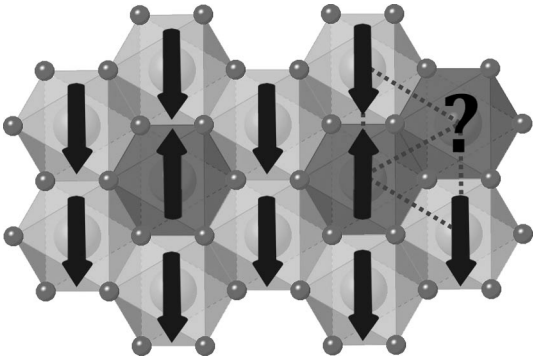

Figure 6. Schematic representation of the occurrence of spin frustration in the studied compounds.

Conclusions

We have synthesized a family of $Ni^{II}Cr^{III}$ layered double hydroxides with the general formula $[Ni^{II}_{3-x}Cr^{III}_{x}(OH)_6](CO_3)_{x/2}\cdot yH_2O$ [x = 0.57 (**1**), 0.69 (**2**), 0.81 (**3**) and 0.93 (**4**)]. The employment of homogeneous precipitation methods allowed for the preparation of large-size hexagonal platelets in good yields. The observed X-ray diffraction patterns account for the purity and crystallinity of the isolated LDH phases. Cationic brucite-like sheets are built up by the intercalation of anionic carbonate anions in all the cases. Subsequently, the interplanar distance is forced to be constant for the whole set of studied compounds (ca. 7.7 Å) in such a way that the extent of interlayer magnetic coupling, promoted by the occurrence of dipolar interactions between long-range correlated ferrimagnetic layers, must be nearly the same. For this reason, differences in the observed magnetic behaviour must arise from the balance between ferro- (Ni^{II}–O–Ni^{II}) and antiferromagnetically (Ni^{II}–O–Cr^{III} and Cr^{III}–O–Cr^{III}) coupled pairs all over the layers for each particular case. Even though Θ values for **1**–**4**, estimated in the high-temperature paramagnetic regime, increase linearly with the Cr^{3+} content along the layers, as expected for the higher ratio of antiferromagnetically coupled Ni–O–Cr and Cr–O–Cr pairs with respect to the ferromagnetic Ni–O–Ni ones, no equivalent trend was observed for the occurrence of spontaneous magnetization. Indeed, T_c values only show a small but not significant variation. Probably, the small variation of the chemical composition allowed in LDH compounds is not enough to lead to more severe effects on the tuning of their magnetic properties. All the studied compounds exhibit spontaneous magnetization at low temperatures as a consequence of their glassy-like ferrimagnetic behaviour. The origin for glassiness in these systems is the combination of competing magnetic interactions and the random distribution of spin carriers (statistical disorder) throughout the cationic layers, which might even promote the appearance of spin frustration.

The dimetallic nature of this sort of layered materials allows for the choice of their metal components at will, thus permitting the tuning of the nature and extent of magnetic exchange along the hydroxyl-supported cationic layers. This point should be very useful in preparing LDH materials that exhibit spontaneous magnetization at higher temperatures. With this in mind, we are currently working on the preparation of new layered magnets of this family along with new hybrid magnets obtained by intercalation of magnetic molecular species in between the magnetic brucite-like sheets.

Experimental Section

Synthesis: All chemicals [$NiCl_2\cdot6H_2O$, $CrCl_3\cdot6H_2O$ and hexamethylenetetramine (HMT = $C_6H_{12}N_4$)] were analytical grade and used as received from Fluka. Typically, nickel chloride and chromium chloride were dissolved in deionized water to yield a total metal cation concentration of 0.15 M and stoichiometric coefficient values, x, ranging from 0.6 to 1. The amount of HMT, three times the [Cr^{3+}] in the synthesis with x = 1 and fixed for all the x values, was then introduced into the solution. The resulting mixture was placed in a Teflon inner vessel within a stainless steel outer vessel. The vessels were placed in a preheated oven at 140 °C, and the mixture was allowed to react under air-tight conditions. After 72 h, the vessels were removed and cooled on a bench to room temperature. The resulting product was filtered and dried in a vacuum. The pH of the initial mixture was around 5 and that of the resulting solution was around 8, depending on the x value.

Physical Characterization: The metal composition of bulk samples was determined by electron probe microanalysis (EPMA) performed in a Philips SEM XL30 equipped with an EDAX micro-

probe. Particles morphologies and dimensions were studied with a Hitachi S-4100 scanning electron microscope at an accelerating voltage of 20 keV. Infrared spectra were recorded with a FTIR Nicolet 5700 spectrometer (4000–400 cm^{-1} range) by using powdered samples in KBr pellets. X-ray powder profiles were collected with a Siemens d-500 X-ray diffractometer (Cu-K_α radiation, λ_α = 1.54184 Å) at 293(2) K. Samples were grounded and mounted on a flat sample plate. Typically, profiles were collected as step scans over a 2.16-h period in the $5° < 2\theta < 70°$ range with a step size of 0.05°. Thermogravimetric measurements were carried out with a Mettler Toledo TGA/SDTA 851 apparatus in the 25–800 °C temperature interval in air and at a 5 K min^{-1} scan rate. Magnetic susceptibility measurements were performed on polycrystalline samples with a Quantum Design PPMS-9 model instrument. The susceptibility data were corrected by removing the diamagnetic contributions as deduced by using Pascal's constant tables. The dc data were collected in the range 2–300 K upon decreasing temperatures with an applied field of 1000 G, and hysteresis loops were collected between –5 and +5 T at 2 K. The ac data were collected in the range 2–30 K with an applied alternating field of 3.95 G at different frequencies in the range 10–10000 Hz.

Supporting Information (see footnote on the first page of this article): additional SEM images, TG and DTA curves, Curie–Weiss fitting of the magnetic data, hysteresis loops, Arrhenius fitting of the out-of-phase maxima employed in the energy barrier estimation, FTIR spectra and assignment of the main vibration modes.

Acknowledgments

Financial support from the European Union (NoE MAGMANet), the Spanish Ministerio de Ciencia e Innovación (Project Consolider-Ingenio in Molecular Nanoscience, CSD2007-00010, and projects MAT2004-03849, MAT2007-61584 and CTQ-2005-09385), and the Generalitat Valenciana are gratefully acknowledged. A. R. thanks the Spanish government for a RyC research contract. Helpful discussions with José R. Galán-Mascarós and the help with the magnetic measurements of José M. Martínez-Agudo are also gratefully acknowledged.

[1] a) F. Cavani, F. Trifirò, A. Vaccari, *Catal. Today* **1991**, *11*, 173–301; b) V. Rives, *Layered Double Hydroxides: Present and Future*, Nova Science Publishers, New York, **2001**; c) A. I. Khan, D. O'Hare, *J. Mater. Chem.* **2002**, *12*, 3191–3198.
[2] a) I. Y. Park, K. Kuroda, C. Kato, *Chem. Lett.* **1989**, *11*, 2057–2058; b) M. Chibwe, T. J. Pinnavaia, *J. Chem. Soc., Chem. Commun.* **1993**, *3*, 278–280.
[3] a) S. K. Yun, T. J. Pinnavaia, *Inorg. Chem.* **1996**, *35*, 6853–6860; b) E. M. Serwicka, P. Nowak, K. Bahranowski, W. Jones, F. Kooli, *J. Mater. Chem.* **1997**, *7*, 1937–1939.
[4] a) J. H. Choy, S. Y. Kwak, J. S. Park, Y. J. Jeong, J. Portier, *J. Am. Chem. Soc.* **1999**, *121*, 1399–1400; b) S. Aisawa, S. Takahashi, W. Ogasawara, Y. Umetsu, E. Narita, *J. Solid State Chem.* **2001**, *162*, 52–62.
[5] J. H. Choy, S. Y. Kwak, J. S. Park, Y. J. Jeong, *J. Mater. Chem.* **2001**, *11*, 1671–1674.
[6] R. Trujillano, M. J. Holgado, F. Pigazo, V. Rives, *Physica B* **2006**, *373*, 267–273.
[7] M. Intissar, R. Segni, C. Payen, J. P. Besse, F. Leroux, *J. Solid State Chem.* **2002**, *167*, 508–516.
[8] a) V. Laget, C. Hornick, P. Rabu, M. Drillon, *J. Mater. Chem.* **1999**, *9*, 169–174; b) V. Laget, C. Hornick, P. Rabu, M. Drillon, R. Ziessel, *Coord. Chem. Rev.* **1998**, *180*, 1533–1553.
[9] a) Z. L. Huang, M. Drillon, N. Masciocchi, A. Sironi, J. T. Zhao, P. Rabu, P. Panissod, *Chem. Mater.* **2000**, *12*, 2805–2812; b) M. Kurmoo, *Chem. Mater.* **1999**, *11*, 3370–3378.
[10] M. Bujoli-Doeuff, L. Force, V. Gadet, M. Verdaguer, K. El Maiki, A. de Roy, J. P. Besse, J. P. Renard, *Mater. Res. Bull.* **1991**, *26*, 577–587.
[11] E. Coronado, J. R. Galán-Mascarós, C. Martí-Gastaldo, A. Ribera, *Chem. Mater.* **2006**, *18*, 6112–6114.
[12] a) S. Miyata, *Clays Clay Miner.* **1980**, *28*, 50–56; b) S. Miyata, A. Okada, *Clays Clay Miner.* **1977**, *25*, 14–18; c) M. A. Drezdzon, *Inorg. Chem.* **1988**, *27*, 4628–4632; d) E. P. Giannelis, D. G. Nocera, T. J. Pinnavaia, *Inorg. Chem.* **1987**, *26*, 203–205; e) N. Iyi, K. Kurashima, T. Fujita, *Chem. Mater.* **2002**, *14*, 583–589.
[13] a) H. Cai, A. C. Hillier, K. R. Franklin, C. C. Nunn, M. D. Ward, *Science* **1994**, *266*, 1551–1555; b) U. Costantino, F. Marmottini, M. Nocchetti, R. Vivani, *Eur. J. Inorg. Chem.* **1998**, *10*, 1439–1446; c) M. Ogawa, H. Kaiho, *Langmuir* **2002**, *18*, 4240–4242; d) M. Adachi-Pagano, C. Forano, J. P. Besse, *J. Mater. Chem.* **2003**, *13*, 1988–1993; e) N. Iyi, T. Matsumoto, Y. Kaneko, K. Kitamura, *Chem. Lett.* **2004**, *33*, 1122–1123; f) L. Li, R. Ma, Y. Ebina, N. Iyi, T. Sasaki, *Chem. Mater.* **2005**, *17*, 4386–4391; g) Z. Liu, R. Ma, Y. Ebina, N. Iyi, K. Takada, T. Sasaki, *Langmuir* **2007**, *23*, 861–867; h) Z. Liu, R. Ma, M. Osada, N. Iyi, Y. Ebina, K. Takada, T. Sasaki, *J. Am. Chem. Soc.* **2006**, *128*, 4872–4880; i) R. Ma, Z. Liu, L. Li, N. Iyi, T. Sasaki, *J. Mater. Chem.* **2006**, *16*, 3809–3813.
[14] M. J. Hernandez-Moreno, M. A. Ulibarri, J. L. Rendon, C. J. Serna, *Phys. Chem. Miner.* **1985**, *12*, 34–38.
[15] a) G. Busca, F. Trifiro, A. Vaccari, *Langmuir* **1990**, *6*, 1440–1447; b) K. Nakamoto, *Infrared Spectra of Inorganic and Coordination Compounds*, Wiley-Interscience, New York, **1970**.
[16] G. Mascolo, O. Marino, *Mineral. Magn.* **1982**, *46*, 136–137.
[17] G. W. Brindley, S. Kikkawa, *Am. Mineral.* **1979**, *64*, 836–843.
[18] I. Pausch, H. H. Lohse, K. Schurmann, R. Allmann, *Clays Clay Miner.* **1986**, *34*, 507–510.
[19] G. Mascolo, O. Marino, *Mineral. Magn.* **1980**, *43*, 619–621.
[20] a) V. R. L. Constantino, T. J. Pinnavaia, *Inorg. Chem.* **1995**, *34*, 883–892; b) P. Bera, M. Rajamathi, M. S. Hegde, *Bull. Mater. Sci.* **2000**, *23*, 141–145.
[21] F. M. Labajos, V. Rives, M. A. Ulibarri, *J. Mater. Sci.* **1992**, *27*, 1546–1552.
[22] M. Taibi, S. Ammar, N. Jouini, F. Fiévet, P. Molinié, M. Drillon, *J. Mater. Chem.* **2002**, *12*, 3238–3244.
[23] E. Coronado, J. R. Galán-Mascarós, C. Martí-Gastaldo, A. Ribera, E. Palacios, M. Castro, R. Burriel, *Inorg. Chem.* **2008**, *47*, 9103–9110.
[24] J. A. Mydosh, *Spin Glasses: An Experimental Introduction*, Taylor & Francis, London, **1993**.
[25] a) W. B. Brickenhorff, B. G. Morin, E. J. Brandon, J. S. Miller, A. J. Epstein, *J. Appl. Phys.* **1996**, *79*, 6147–6179; b) W. E. Buschmann, J. S. Miller, *Inorg. Chem.* **2000**, *39*, 2411–2421.

Received: July 1, 2008
Published Online: November 21, 2008

